Soft Matter

PAPER

View Article Online
View Journal | View Issue

Cite this: *Soft Matter*, 2024, **20**, 6023

Foam coarsening in a yield stress fluid†

Alice Requier, *[a] Chiara Guidolin, ‡[a] Emmanuelle Rio, [a] Nicolò Galvani, [bc] Sylvie Cohen-Addad, [bd] Olivier Pitois [c] and Anniina Salonen *[a]

Received 8th March 2024,
Accepted 24th June 2024

DOI: 10.1039/d4sm00296b

rsc.li/soft-matter-journal

Foams coarsen because of pressure differences between bubbles of different sizes. We study the coarsening of quasi-2D foams made from model yield stress fluids: concentrated oil-in-water emulsions. We show that increasing the yield stress of the foamed emulsion continuous phase leads to both slower coarsening and irreversible structural change. The impact of the continuous phase rheology is stronger when the foamed emulsion is wetter or more confined. The bubble growth and organisation both become highly heterogeneous with an excess of small bubbles. We present a model that rationalises the impact of these three parameters by taking into account a resisting pressure required to displace the yield stress fluid around the bubbles.

1 Introduction

Liquid foams are dense dispersions of gas bubbles within a continuous liquid phase. Their structure and stability mainly depend on bubble size and liquid volume fraction $\varepsilon = V_{liq}/V_{foam}$ (with V_{liq} the volume of liquid contained in a foam volume V_{foam}). Depending on the foam liquid fraction, bubbles can either be spherical, moving freely in the liquid medium, or polyhedral and in contact. In the latter configuration, bubbles are compressed together and separated by thin liquid films, connected three by three through liquid channels called Plateau borders. Surfactants, which adsorb at the gas–liquid interfaces, are required to produce a stable foam. Yet liquid foams are still fragile materials that irreversibly evolve in time. Three possibly entangled mechanisms alter their structure and eventually lead to foam destabilisation: gravitational liquid drainage, bubble coalescence and foam coarsening.[1] Pioneering foam ageing experiments performed with dry horizontal quasi-2D foams (single monolayers of confined bubbles) showed that this configuration allows neglecting gravitational drainage during the foam evolution.[2] Moreover, the rupture of the liquid films between bubbles, causing bubble coalescence, can be minimised using a surfactant that generates stable films.[1] This means that working in the quasi-2D geometry allows to specifically study foam coarsening.

Foam coarsening is a process driven by Laplace pressure differences between bubbles of different sizes, that cause gas transfer from smaller to larger bubbles. This mechanism leads to a decrease in the number of bubbles with time along with growth of the average bubble size. Coarsening bubble dispersions eventually reach a scaling state where the bubble growth becomes statistically self-similar. All dimensionless geometrical and topological distributions become time invariant, and the average bubble size $\langle R \rangle$ grows in time as a power law $\langle R \rangle \sim t^{\alpha}$, where α depends on the mechanism of gas transfer between bubbles. For dry foams, *i.e.*, with small liquid fraction, gas diffusion through liquid films dominates and theory predicts that the mean bubble size evolves with time as $\langle R \rangle \sim t^{1/2}$.[3–5] This prediction is experimentally verified for the limiting case of a very dry foam $\varepsilon \sim 1\%$.[6,7] This coarsening law is also derived in a 2D configuration[8] and measured in quasi-2D foams.[9,10]

Liquid foams exhibit unusual mechanical properties based on their typical cellular structure and the rearrangement dynamics of the bubbles.[11–15] Combined with their lightness and high interfacial area, this makes them interesting for many personal and industrial applications, including cosmetics, oil recovery, pharmaceutics and food industry. In many of these applications, the foam continuous phase is a complex fluid with non-Newtonian rheology.[16] These materials may exhibit a threshold in applied stress, called the yield stress, below which they behave like solids, and above which they flow. Foaming such fluids can be beneficial as they can improve foam stability and change their rheology.[17,18] A yield stress fluid can prevent entrapped bubbles from rising,[19,20] or stop coarsening.[21]

[a] *Université Paris-Saclay, CNRS, Laboratoire de Physique des Solides, 91405 Orsay, France. E-mail: anniina.salonen@universite-paris-saclay.fr*
[b] *Sorbonne Université, CNRS-UMR 7588, Institut des NanoSciences de Paris, 4 Place Jussieu, 75005 Paris, France*
[c] *Université Gustave Eiffel, ENPC, CNRS, Laboratoire Navier, 5 Bd Descartes, Champs-sur-Marne, F-77454 Marne-la-Vallée Cedex 2, France*
[d] *Université Gustave Eiffel, 5 Bd Descartes, Champs-sur-Marne, F-77454 Marne-la-Vallée Cedex 2, France*

† Electronic supplementary information (ESI) available. See DOI: https://doi.org/10.1039/d4sm00296b

‡ Present address: Department of Medical Biotechnology and Translational Medicine, University of Milan, Segrate, Italy.

Moreover, most solid foams are made from fluid precursors, which are subsequently solidified, hence the continuous phase passes through a variety of stages of rheological behaviour. Bubbles in materials result in lighter foams and better insulating properties,[22] but their presence can also be detrimental, as trapped bubbles may negatively affect material physical properties.[23]

Emulsions are good candidates of non-Newtonian fluids to foam. Different types of foamed emulsions exist, depending on the continuous phase surrounding the bubbles: the latter can be either a water-in-oil emulsion, an oil-in-water emulsion or even a bi-continuous oil and water phase.[24] Dispersions of bubbles in mixtures of oil and water, stabilised by particles rather than surfactants, are also widely studied.[25,26] In particular, highly concentrated oil-in-water emulsions are a good example of yield stress fluids. Previous studies have shown that swapping a foam aqueous phase for an emulsion dramatically changes its behaviour and properties,[27,28] and in particular the emulsion yield stress can be high enough to stop foam gravitational drainage, making very stable foams.[29] The coarsening of single bubbles is also expected to slow down or stop in complex fluids.[30,31] The study of bubbles suspensions in silicone oil-in-water emulsions also showed that their rheological behaviour depends on the stress applied to the sample: the coupling between bubble deformation and bulk rheology is different whether the emulsion yields or not.[32] All this work suggests that the ageing undergone by the trapped bubbles may be impacted by the rheology of the foam continuous phase.

In this paper, we study coarsening of quasi-2D foamed emulsions. The continuous phase is a concentrated oil-in-water emulsion, which is a model yield stress fluid. We have recently shown that foams made from emulsions with high oil volume fractions ϕ coarsen more slowly and evolve into highly heterogeneous structures.[28] In this work we explore the effect of varying the foamed emulsion liquid fraction ε and the confining gap d on its ageing and we rationalise the impact of ϕ, ε and d on the foamed emulsion structure and evolution. To do so, we follow the evolution of the average bubble radius and the bubble size distributions with time.

2 Materials and methods

2.1 Emulsion generation

Concentrated oil-in-water emulsions with varying oil volume fractions are prepared by mixing the freshly-made aqueous phase, composed of sodium dodecyl sulfate (SDS, Sigma Aldrich) at 30 g L^{-1}, and deionised water (Purelab, resistivity 18.2 MΩ cm), with oil (rapeseed oil from Brassica Rapa or sunflower oil from Helianthus Annuus, Sigma Aldrich) with the double-syringe method.[33] Syringes in polypropylen with a 60 mL volume (Codan, VWR) are connected with a double Luer Lock junction (VWR) and the emulsion is generated by pushing the aqueous and the oil phase back and forth through the connector thirty times at constant velocity. The oil fraction $\phi = V_{oil}/V_{cp}$ (with V_{oil} the volume of oil dispersed in the emulsion volume V_{cp}) ranges between 70% and 85%.

2.2 Emulsion characterisation

The size and polydispersity of the emulsion drops are measured using laser diffraction granulometry with a Mastersizer 3000E (Malvern Panalytical) equipped with a Hydro SM wet dispersion unit. The surface-weighted mean drop diameter decreases slightly from 5 to 2 μm with increasing ϕ up to 85%.

The rheological properties of the emulsions are measured with a rheometer (MCR 302, Anton Paar) using a cylindrical Couette geometry (CC27, Anton Paar). The surface of the measuring tool has been sand-blasted to ensure a no-slip condition for the measurement. Oscillatory strain sweep tests are performed increasing the strain amplitude from 10^{-3}% to 10^{2}% at a constant frequency of 1 Hz. The gap width is equal to 1.1 mm and the temperature is set to (20.5 ± 0.5) °C. The storage and loss moduli, G' and G'' are determined in the limit of small strain amplitude. The stress *versus* strain amplitude curves also give access to the emulsion yield stress τ_y by determining the cross-over between the linear regime at low strain and the non-linear regime at high strain. The emulsion storage modulus varies from 114 to 506 Pa and the yield stress from 1 to 23 Pa as ϕ increases from 70% to 85%. We note that the average droplet size also varies as ϕ changes. The ϕ-dependence of G', G'', and τ_y is shown in Fig. 1. The storage modulus and yield stress follow the classical scalings $G' \sim \phi(\phi - \phi^\star)\gamma/r$[34] and $\tau_y \sim (\phi - \phi^\star)^2\gamma/r$,[35] which are shown in Fig. S1 in ESI.† Fig. 1 (circles) show that the rheological parameters of emulsions made with sunflower oil are similar to the ones of emulsions made with rapeseed oil (squares).

2.3 Foam generation

The emulsion is foamed using a planetary kitchen mixer (Kenwood KMIX750AW, 1000 W). The double rotation of the whisk slowly entraps air pockets in the continuous phase.[36] The final liquid (emulsion) fraction ε can be controlled by adjusting the mixing protocol: gradually increasing the mixing speed up to the maximum level along with a long mixing time (around

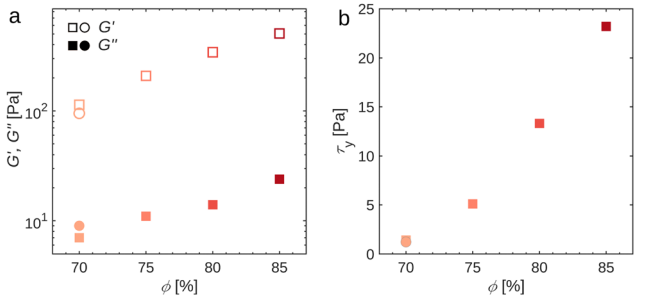

Fig. 1 Evolution of (a) the storage (empty markers) and loss (solid markers) moduli, respectively called G' and G'', as well as (b) the yield stress τ_y of the emulsion, depending on its oil fraction. At high ϕ the emulsion is a viscoelastic yield-stress fluid. Squares refer to samples made with rapeseed oil, circles to sunflower oil samples.

Table 1 Experimental parameters of the different foamed emulsions studied. One line is one sample, defined by its oil fraction ϕ, liquid fraction ε, and the gap between the plates d. t_0 is the time at which the foamed emulsion structure becomes 2D and $\langle R_0 \rangle$ and $\mu^R_{3,0}$ the values of respectively the average radius and third moment of the bubble size distribution at that time

ϕ [%]	ε [%]	d [mm]	t_0 [h]	$\langle R_0 \rangle$ [mm]	$\mu^R_{3,0} \times 10^{-2}$
0	10	1	2.3	0.89	4.8
70	10	1	3.0	0.89	2.6
75	10	1	3.2	0.88	3.2
80	10	1	3.6	0.98	3.2
85	10	1	5.1	0.82	3.1
70	9	1	2.6	0.89	7.8
70	13	1	3.8	0.84	3.6
70	20	1	5.3	0.85	2.4
70	25	1	6.9	0.85	3.9
75	25	1	7.6	0.87	0.5
80	25	1	7.7	0.91	0.9
80	10	1	3.2	1.07	5.7
80	10	2	8.0	1.52	2.9
80	10	3	15.8	2.20	2.4

35 minutes) leads to foams at $\varepsilon \simeq 9\%$, whereas mixing for less time at low speed leads to wetter ones. The liquid fraction is measured by weight immediately after foam generation and ranges between 9% and 25%. The different samples studied are listed in Table 1. Experiments where we vary the liquid fraction are made with sunflower oil. The oil drop size distribution is measured after foaming and after the end of the coarsening experiments.[28] It is unchanged from the original distribution, therefore the emulsion is stable throughout the foam generation and ageing process.

2.4 Foam coarsening experiments

Once the foamed emulsion is prepared, it is squeezed between two transparent horizontal glass plates. The plates are square with 24 cm sides, and they are separated by a rubber seal of thickness d. We measure the resulting gap between the plates, and find that it corresponds to d within 10% uncertainty. Most of the experiments are done with $d = 1$ mm, however the impact of d has been tested using $d = 2$ or 3 mm. The plates are fixed between two duralumin frames. The cell is illuminated from above by a square of LED lights and placed under a high-resolution camera (Basler acA3800 – 14 um, 3840 × 2748 pixels) equipped with a lens (Fujinon 16 mm f/1.4).

We let the foam coarsen and we follow its evolution over time by recording a photograph every 3 or 5 minutes at the early stages and every 30 minutes or one hour at later stages. At very early times, the foam exhibits a 3D structure and multi-layers of small bubbles can be observed in the cell. After a certain time, that we call t_0, as the foam coarsens most of the bubbles in the foam become larger than the gap d and we have a monolayer of bubbles. The average bubble radii $\langle R_0 \rangle = \langle R(t = t_0) \rangle$ and times t_0 are summarised in Table 1 for the different samples. We can note that $\langle R_0 \rangle$ are slightly smaller than the gap size, indicating that the bubble diameters are almost twice the gap width. This ensures that in the polydisperse bubble size distribution most of the bubbles are indeed quasi-2D. All of the presented results refer to the regime $t \geq t_0$.

In addition, to test whether the mechanical boundary condition has an effect on the coarsening dynamics in our confined geometry, we carried out an experiment where the glass plates have been previously roughened with glass beads, leading to a roughness depth around 30 μm. For this test, we use a foamed emulsion with $\phi = 70\%$ and $\varepsilon = 13\%$, confined within a gap $d = 1$ mm.

2.5 Image analysis

Custom Matlab scripts are used to analyse the photographs. A first pre-treatment, in which the raw pictures are cropped and contrast-adjusted, is necessary to get a proper image segmentation. The foam skeleton is then obtained from the segmented pictures through a watershed algorithm. The latter is detected to be in the middle of the foam Plateau borders, no matter their thickness. The area A of each polygonal bubble is then retrieved using the built-in function regionprops. The bubble equivalent radius is then calculated as $R = \sqrt{A/\pi}$.

3 Results and discussion

We have studied the effects of changing the emulsion oil fraction ϕ, the foam liquid fraction ε and the gap between the glass plates d on the different features of the foam.

3.1 Foam evolution during coarsening

Photographs of an aqueous foam and three foamed emulsions, together with the corresponding bubble size distributions, are shown in Fig. 2 for different foam ages. The times chosen are t_0, the time at which the foam structure becomes 2D, t_0 + 72 h and t_f, the time of the last recorded photograph. We chose t_0 + 72 h as the foams have evolved, but this instant does not coincide with the end of the measurement for any of the foams.

The top row (a–c) shows the temporal evolution of a dry aqueous foam made from an SDS solution and with a liquid fraction of $\varepsilon = 10\%$. We see that in time, the bubble size increases and the number of bubbles decreases. We observe the typical cellular structure of a 2D dry aqueous foam. This means polygonal bubbles packed together with a characteristic local equilibrium structure. The bubble size distributions, represented as a function of the normalised radius $R/\langle R \rangle$, are shown in Fig. 2d. They are invariant in time, as it has been observed in quasi-2D foams with similar liquid fractions.[37]

The second row (e–g) shows the structural evolution of a dry foamed emulsion ($\varepsilon = 10\%$ and $\phi = 70\%$). As for the aqueous foam, the bubble size increases with time while the number of bubbles decreases. If we compare the foamed emulsion structure to the one of the aqueous foam, the photographs look alike. However, a closer look reveals some tiny bubbles and a hint of heterogeneity in the Plateau border thicknesses in the foamed emulsion (g) that we do not see in the aqueous foam (c). The bubble size distribution (h) at t_f is also a bit different, as it has become slightly triangular with a peak that has shifted towards the left compared to the initial distribution.

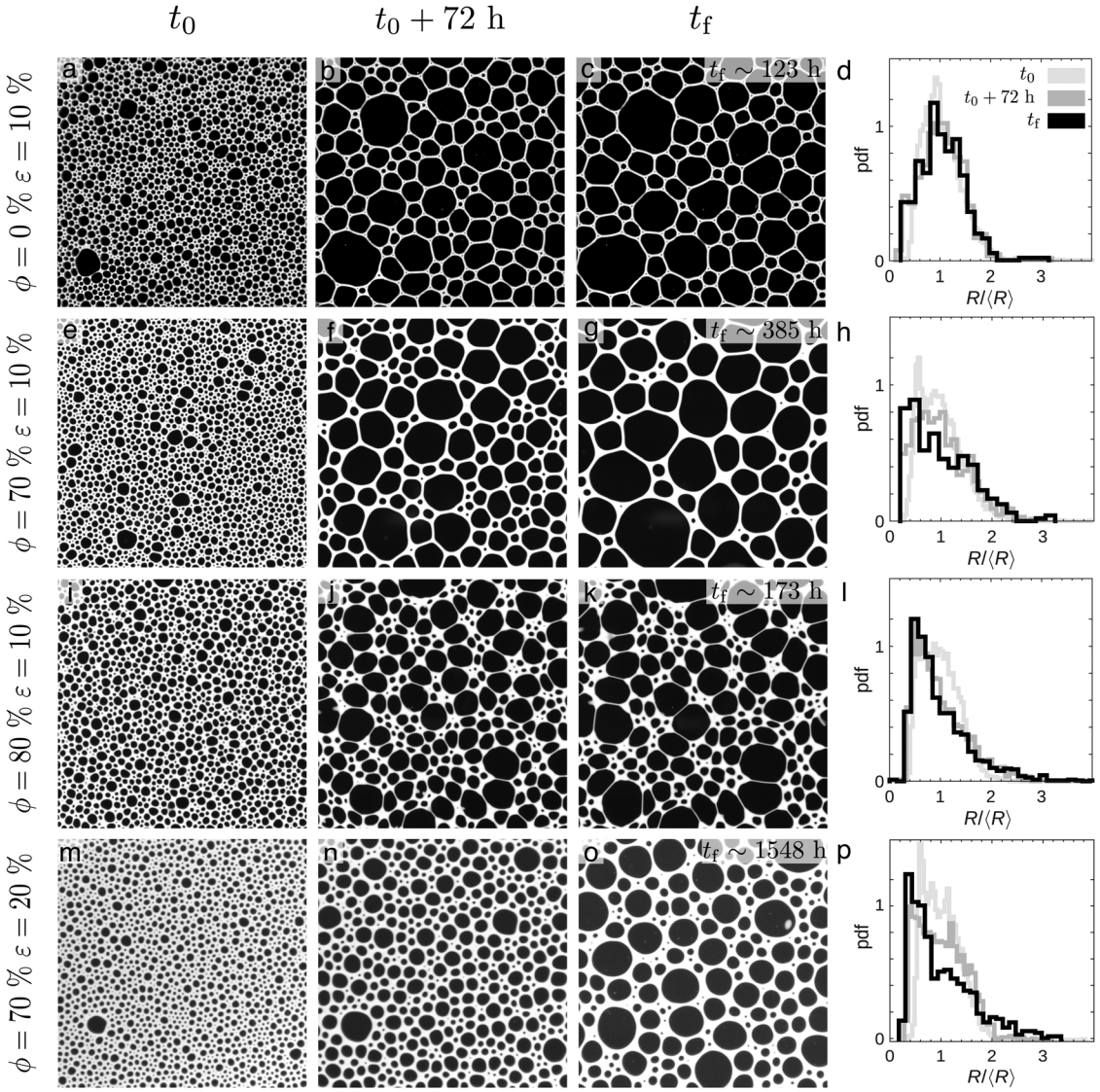

Fig. 2 Photographs of foams at three different times and the corresponding bubble size distributions for an aqueous foam (a)–(d) and foamed emulsions (e)–(p). Top line (a)–(c) shows photographs of a dry SDS foam with ε = 10% liquid. Second line (e)–(g) corresponds to a dry foamed emulsion: ε = 10% and ϕ = 70%. Third line (i)–(k) is a dry foamed emulsion (ε = 10%) with a more viscoelastic continuous phase (ϕ = 80%). Bottom row (m)–(o) corresponds to a wet foamed emulsion with ε = 20% and ϕ = 70%. For each foam, time increases in the photographs from left to right: t_0 the time at which the foam structure becomes quasi-2D, three days later and t_f the time of the last recorded photograph. The values of t_0 are given in Table 1. The instants t_f are shown on photographs (c), (g), (k) and (o). Edge of the photographs is 70 mm. The last column on the right shows the bubble size distributions, represented as a function of the normalised radius $R/\langle R \rangle$, corresponding to each sample: the pale grey is at t_0, dark grey at t_0 + 72 h and black at t_f.

Photographs of the third row (i–k) show the evolution of a dry foamed emulsion (ε = 10%) with a higher oil fraction in the continuous phase (ϕ = 80%) and thus with a higher yield stress and elastic modulus (*cf.* Fig. 1). This time the foamed emulsion structure at t_0 (i) looks different compared to the one at ϕ = 70% (e), even though the bubble size distributions (pale grey, h and l) are similar. We start to see hints of the impact of the oil with the apparition of peculiar features, such as elongated bubble shapes. The effect of high ϕ is clearly visible when it comes to $t = t_0$ + 72 h (photograph j). Not only are the bubbles smaller than in the other foams but the bubble organisation is also very different between f and j. Indeed for ϕ = 80% a structural heterogeneity becomes visible with two populations of bubbles: big ones, separated by very thin Plateau borders, and localised areas of very small bubbles surrounded by much more liquid. This suggests that the liquid is not distributed within the foam during coarsening. Finally, the photograph at t_f (k) shows a foamed emulsion that is very similar to photograph (j) even though separated in time by a hundred hours. The coarsening process is significantly slowed down, and specifically the small bubbles seem to linger. This excess of small bubbles within the foam becomes visible in the bubble size distributions in (l). The distributions become increasingly asymmetric and the peak shifts left with time, meaning it is shifted towards smaller bubbles.

Finally, the bottom row shows the impact of increasing liquid fraction on the evolution of a foam with ϕ = 70%

(m–o). A higher liquid fraction (ε = 20%) results in slower coarsening, and the bubbles are much smaller at t_0 + 72 h (n) when compared to the sample at ϕ = 70% and ε = 10% (f). Although t_f is much larger at 1548 h in (o) *versus* 385 h in (g), the final bubble sizes are much smaller. In this last sample we can also notice the accumulation of small bubbles which is confirmed by the shape of the bubble size distributions at long times in (p).

We observe the slowing down of coarsening, and changes in the foam structure with increased oil volume fraction. A higher foam liquid fraction amplifies the impact of the emulsion.

3.2 Temporal evolution of bubble size and skewness

In order to quantify the temporal evolution of the foams, we measure the average bubble size $\langle R\rangle$. Fig. 3a and b show the evolution of the normalised average bubble radius $\tilde{R} = \langle R\rangle/\langle R_0\rangle$, where $\langle R_0\rangle = \langle R(t_0)\rangle$, as a function of normalised time t/t_0. Fig. 3a shows the effect of varying the oil fraction ϕ at constant liquid fraction (ε = 10%). The pale blue crosses represent the evolution of $\tilde{R}$ with the normalised time for an aqueous SDS foam with ε = 10%. The average radius of the aqueous foam evolves with something resembling a power law, with an exponent close to 1/3, which starts to flatten out at longer times. This is in contrast to dry aqueous foams in 2D or 3D, which should evolve as $\tilde{R} \sim t^{1/2}$.[7,38] Indeed we do not expect a power-law coarsening due to the quasi-2D geometry of the foam. As the bubble size increases, the Plateau borders thicken.[39] The increase in the Plateau borders radius r_{PB} results in a decrease of the height of the contact film between bubbles $h = d - 2r_{PB}$ (d being the gap between the plates). The induced reduction in thin film area leads to a border-blocking effect which slows down gas transfer, thus resulting in a lower coarsening rate.[37] Therefore, the growth of an even moderately wet quasi-2D aqueous foam does not follow the 1/2 power law.[40,41]

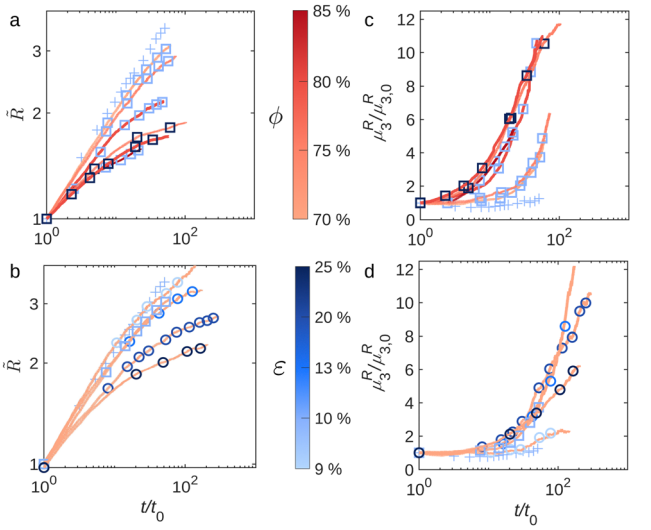

Fig. 3 Left: Evolution of the normalised average bubble radius $\tilde{R} = \langle R\rangle/\langle R_0\rangle$ with t/t_0 for (a) samples with liquid fraction ε = 10% (pale blue) or ε = 25% (navy blue) and oil fraction ϕ ranging between 70% (pale orange) and 85% (brick red) and (b) samples with oil fraction ϕ = 70% and liquid fraction ε ranging from 9% (pale blue) to 25% (navy blue). The coarsening slows down as the foamed emulsion is wetter and/or as the continuous phase is more viscoelastic. Right: Evolution of $\mu_3^R/\mu_{3,0}^R$ ($\mu_{3,0}^R = \mu_3^R(t_0)$) with t/t_0 for the same samples with: (c) varying oil fraction and (d) varying liquid fraction. The pale blue crosses show the evolution for an SDS foam with ε = 10%. The steep increase of μ_3^R for foamed emulsions differs from aqueous foam behaviour. Squares refer to emulsions made with rapeseed oil and circles to ones with sunflower oil.

We now have a look at the bubble size evolution in foamed emulsions with increasing oil volume fraction ϕ, shown in Fig. 3a. We can see the effect of varying the elastic modulus G' and the yield stress τ_y of the continuous phase since both are increasing functions of ϕ (*cf.* Fig. 1). We notice that as ϕ increases the bubble growth becomes weaker and the growth rate at early times decreases. The higher ϕ, the earlier $\tilde{R}$ starts to flatten. This suggests that the presence of emulsion strongly affects the bubble growth and significantly slows down the coarsening process.

For its part, Fig. 3b shows the effect of varying the foam liquid fraction ε keeping the oil fraction constant (at ϕ = 70%). The pale blue crosses still represent $\tilde{R}(t/t_0)$ for the aqueous SDS foam with ε = 10%. We saw that the presence of oil in the foam continuous phase contributes to slow down the coarsening process and Fig. 3b shows that increasing ε amplifies this effect. This is confirmed by the decrease of the growth rate and the flattening of $\tilde{R}$ at an earlier time with increasing ε: a wetter foamed emulsion coarsens significantly more slowly, consistent with what is shown in the photographs in Fig. 2f and n.

We saw in Fig. 2(d), (h), (l) and (p) that in contrast to aqueous foams, the normalised bubble size distributions for the foamed emulsions vary in time. They become highly asymmetrical and develop a peak at small $R/\langle R\rangle$, reflecting an excess of small bubbles within the foam. A recent study of 3D aqueous foam coarsening revealed an excess of small bubbles roaming in the interstices between bigger jammed bubbles within the foam in the scaling state.[42] However here the observed excess of small bubbles has a different origin since it results from their shrinkage slowdown due to a thick layer of emulsion surrounding them. There are different ways to quantify the change in the distributions shape along the coarsening. A first method based on the shift of the distribution peak is described in ESI.† Here, we quantify this change using the bubble size distribution third moment $\mu_3^R = \left\langle \left(\frac{R}{\langle R\rangle} - 1 \right)^3 \right\rangle$, which is sensitive to its asymmetry. For an aqueous foam in the scaling state, μ_3^R is constant in time and its value depends on the liquid fraction of the foam.[43] By contrast, in the foamed emulsions μ_3^R starts off constant, but deviates at a certain time, as seen in Fig. 3c and d, where the normalised third moment $\mu_3^R/\mu_{3,0}^R$ (with $\mu_{3,0}^R = \mu_3^R(t_0)$) is shown as a function of t/t_0. The two methods give comparable results as seen in Fig. S2 and S5 of ESI† and we choose to continue with $\mu_3^R(t)$.

We plot the normalised third moment $\mu_3^R/\mu_{3,0}^R$ as a function of t/t_0 for samples with varying oil fraction at ε = 10% and ε = 25% (Fig. 3c) and for samples with a fixed oil fraction ϕ = 70%

and varying liquid fraction (Fig. 3d). The pale blue crosses in both graphs still represent the evolution of normalised μ_3^R with normalised time for an aqueous SDS foam with $\varepsilon = 10\%$. Values of $\mu_{3,0}^R$ for the different experiments are given in Table 1. We observe that the third moment of foamed emulsion systematically departs from its initial plateau after a certain time, which depends on the sample. The steep increase of μ_3^R is evidence that these foamed emulsions are not evolving towards a self-similar regime. The shift of the bubble size distribution peak due to the accumulation of the small bubbles, observed for these samples in Fig. 2(h), (l) and (p) is responsible for the significant rise of the third moment μ_3^R.

3.3 Evolution of $\mu_3^R(R)$

We saw that in all the foamed emulsions μ_3^R departed from its constant value during the coarsening process. The average bubble size sets the average Laplace pressure difference between the bubbles, and hence the coarsening rate. For this reason, we plot now the evolution of μ_3^R, not as a function of t, but as a function of $\langle R \rangle$.

By plotting the normalised $\mu_3^R/\mu_{3,0}^R$ as a function of the average bubble radius $\langle R \rangle$ (*cf.* Fig. 4), we can also observe its departure from an initial plateau for all foamed emulsions. The higher ϕ and the higher ε, the smaller the average bubble size at which the skew deviates. For example, for a foamed emulsion with $\phi = 70\%$ and $\varepsilon = 10\%$, $\mu_3^R/\mu_{3,0}^R$ deviates at a radius around 2 mm. If the foamed emulsion is wetter ($\phi = 70\%$ and $\varepsilon = 20\%$), it deviates at around 1.4 mm. Finally, for a continuous phase with a higher yield stress and elastic modulus ($\phi = 80\%$ and $\varepsilon = 10\%$), the radius at which we observe the deviation of $\mu_3^R/\mu_{3,0}^R$ is close to 1 mm. We define an experimental critical radius as the average radius at which $\mu_3^R/\mu_{3,0}^R$ has increased by 50% from its plateau (corresponding to $\mu_3^R/\mu_{3,0}^R = 1$) and call it R_{sk}. Therefore,

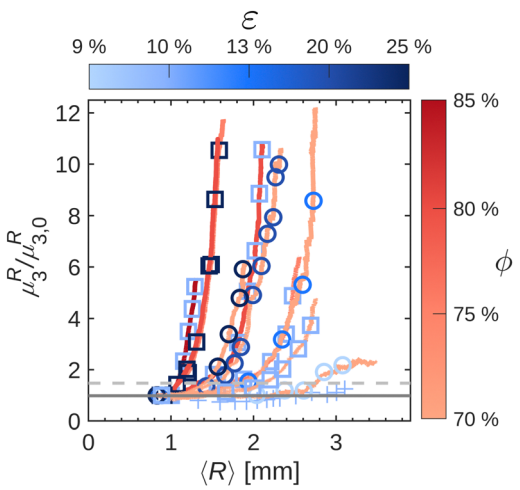

Fig. 4 Normalised third moment of the bubble radius distributions $\mu_3^R/\mu_{3,0}^R$ ($\mu_{3,0}^R = \mu_3^R(t_0)$) plotted as a function of the average bubble size $\langle R \rangle$. The evolution is shown for all the samples in Fig. 3 with the same symbols. The solid grey line shows the initial average plateau at early times. The dashed grey line indicates 150% of this value; R_{sk} is found by the intersection between the curves and the dashed line.

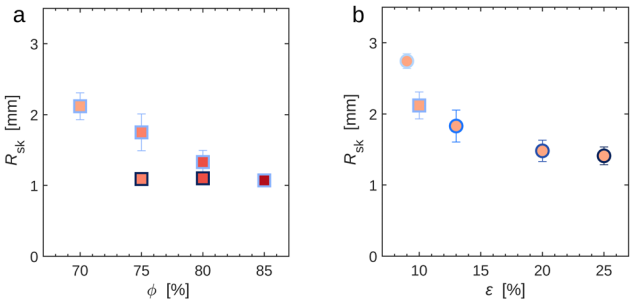

Fig. 5 Values of the experimental critical bubble radius R_{sk} depending on (a) the emulsion oil fraction ϕ and (b) the foamed emulsion liquid fraction ε. R_{sk} gets smaller as the foamed emulsion is wetter and/or the foam continuous phase is plastic. Squares refer to samples made with rapeseed oil, circles to sunflower oil samples.

R_{sk} is, by construction, a relative parameter which enables us to identify the characteristic average radius at which the foamed emulsion behaviour has deviated from the one of aqueous foam.

The values of R_{sk} for all samples studied are plotted in Fig. 5. Fig. 5a shows the evolution of R_{sk} as a function of the emulsion oil fraction ϕ and Fig. 5b represents R_{sk} *vs.* the foam liquid fraction ε. Note that an uncertainty is given for each value of R_{sk}, coming from Fig. 4 taking 120% and 180% of the initial plateau instead of 150%. It is worth noticing that a difference of about 15% can be found in the value of R_{sk} for the same experiment repeated twice. We find that R_{sk} systematically decreases with increasing ϕ (and so with increasing G' and τ_y, see Fig. 1a and b) and ε. This means that the accumulation of small bubbles within the sample, as well as the foam structure change, happen at smaller average radii as the yield stress of the emulsion gets higher (increasing ϕ) or the amount of the yield stress fluid in the foam increases (increasing ε). The impact of foam confinement on the evolution of $\mu_3^R/\mu_{3,0}^R$ with $\langle R \rangle$ is also studied using $d = 2$ and $d = 3$ mm. Increasing the gap between the plates results in an increase of R_{sk}: the larger the confining gap, the larger the average radius at which small bubbles accumulate. Results are shown in Fig. S3 and S5 of ESI.†

3.4 Impact of emulsion on local foam structure

We can summarise the impact of the continuous fluid on the evolution of the foamed emulsions as follows: (1) the growth of the average bubble radius slows down compared to aqueous foams, (2) the shrinkage of smaller bubbles slows down, making them accumulate, and leading to a visible impact on the bubble size distribution once $\langle R \rangle \sim R_{sk}$ and (3) the foamed emulsion structure exhibits unusual bubble patterns at high ϕ.

Let us have a closer look to what happens to the foamed emulsion at early times and describe qualitatively how it evolves. The foam is very polydisperse as we make it, so smaller and larger bubbles coexist (see left column in Fig. 2). As part of the coarsening process smaller bubbles transfer their gas to larger ones, shrink and eventually disappear. Fig. 6 shows photographs of an aqueous foam ($\varepsilon = 10\%$, top row) and a

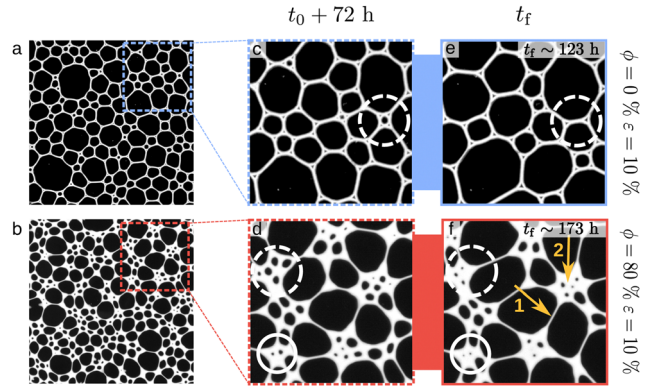

Fig. 6 Photographs of an aqueous foam (top row) (ε = 10%) and foamed emulsion (bottom row) (ϕ = 80%, ε = 10%) during the coarsening process. Left column (a) and (b) shows pictures taken at $t = t_0 + 72$ h, with t_0 the time at which the foam structure becomes 2D (see Table 1). Edge is 70 mm. Middle column (c) and (d) shows zoomed photographs of (a) and (b). Zoomed photographs taken at the final time of the experiment t_f are shown in right column (e) and (f). Edge of zoomed photographs is 29 mm. White dashed circles in (c)–(f) point out bubbles disappearing during the coarsening in an aqueous foam (c) and (e) and in a foamed emulsion (d) and (f). White solid circles in (d) and (f) show bubbles shrinking extremely slowly. Finally yellow arrows in photograph (f) show the heterogeneity in the Plateau border thickness in a foamed emulsion: 1 points out a very thin Plateau border separating two big bubbles and 2 a cluster of tiny bubbles surrounded by much more liquid.

foamed emulsion (ϕ = 80%, ε = 10%, bottom row) during the coarsening process. We observe in photographs c–f a global increase of the bubble size with time and the disappearance of smaller bubbles. However, we want to concentrate on the local organisation of the bubbles during the coarsening. In the aqueous foam, when a bubble disappears the liquid is redistributed and the bubbles rearrange to return to the equilibrium foam structure (see Fig. 6c and e, white dashed circle).[1] By contrast, in the foamed emulsion when small bubbles disappear they leave behind the emulsion that surrounded them and the bubbles do not reorganise (see Fig. 6d and f, white dashed circle, where bubbles are replaced by white patches of emulsion). Thus, as the small bubbles disappear, a progressive thickening of the emulsion layers is observed in localised areas of the foamed emulsion. Bubbles that have not already disappeared are then surrounded by more emulsion, and at a certain point the foam structure becomes highly heterogeneous. This structural heterogeneity is visible in Fig. 6f, where two populations of bubbles coexist: big ones, separated by very thin Plateau borders (Fig. 6f yellow arrow 1), and localised areas of very small bubbles surrounded by more liquid (Fig. 6f yellow arrow 2). This is in contrast to the aqueous foam, in which the Plateau borders have very similar thicknesses (Fig. 6e). This heterogeneity in the foam structure is associated with heterogeneous foam growth. Indeed, the shrinkage of smaller bubbles is significantly slowed down by the stiffness of the thick zones of emulsion they are embedded in, while the bigger bubbles keep coarsening. Fig. 6d and f (white solid circle) show an example of two bubbles slowly shrinking for about a hundred hours. The coarsening process is hindered by the rheology of the emulsion that is not redistributed. In the following part, we build a model to formalise these experimental observations.

3.5 Model for hindered foam coarsening

We propose a simplified model for foamed emulsion coarsening to extract a critical radius at which the emulsion rheology hinders the foam coarsening process, and compare it with the experimental one R_{sk}.

First, to describe why the small bubbles dissolve so slowly into the larger bubbles, we consider the Laplace pressure difference between small bubbles and big ones, that is the driving force of the gas transfer:[44]

$$\Delta P_L \sim \frac{\gamma}{\langle R \rangle}, \quad (1)$$

where γ is the surface tension and $\langle R \rangle$ is the average bubble radius.

We model the regions of foam with high liquid fraction as consisting of bubbles surrounded by an elastic shell composed of emulsion with yield stress τ_y. We consider that an extra pressure ΔP_y is then required for a bubble to change size (grow or shrink) and to make the shell made of emulsion flow. We assume that the shell is a ring with width ℓ that has uniform mechanical properties. To induce the flow of the shell between the two plates, the stress at the plate (where it reaches its maximum value in the gap) must be larger than the yield stress. Thus the extra pressure can be obtained from the force balance (at yield) by assuming no-slip condition at walls:

$$2\pi R d \Delta P_y \approx 2 \times (2\pi R \ell)\tau_y, \quad (2)$$

leading to the following scaling:

$$\Delta P_y \sim \tau_y \frac{\ell}{d}. \quad (3)$$

It is worth noticing that (1) τ_y is the yield stress of the emulsion even if small bubbles are embedded in the shell, according to results obtained in 3D.[32] We recall that the emulsion yield stress depends on its oil fraction and droplet size, as reported in Fig. 1. (2) As mentioned in Section 2.4, additional experiments have been made using rough surfaces to check that the emulsion does not slip at contact with the plates. Results are shown in Fig. S4 and S5 in ESI† and confirm this no-slip condition, justifying the use of eqn (2).

With such an excess stress, the pressure difference for gas transfer from smaller to larger bubble becomes:

$$\Delta P = \Delta P_L - \Delta P_y. \quad (4)$$

We want to find an expression for the radius at which foamed emulsion rheology starts hindering the coarsening process, *i.e.* the radius at which the emulsion yield stress slows down the foam evolution. To do so we study the point at which both pressure contributions are equal, meaning the point at which the yield stress pressure gets comparable to the Laplace pressure. Considering $\Delta P = 0$ and making eqn (4) dimensionless by

dividing by $\gamma/\langle R_0\rangle$, we obtain:

$$\frac{1}{\tilde{R}} \sim \frac{\tau_y\langle R_0\rangle}{\gamma}\frac{\ell}{\langle R_0\rangle}\frac{\langle R_0\rangle}{d} \sim \mathrm{Bi}\tilde{\ell}\frac{\langle R_0\rangle}{d}, \tag{5}$$

where $\tilde{R} = \langle R\rangle/\langle R_0\rangle$, $\tilde{\ell} = \ell/\langle R_0\rangle$ and $\mathrm{Bi} = \tau_y\langle R_0\rangle/\gamma$ is the Bingham capillary number.

We expect the width ℓ to increase with the number of bubbles that have disappeared around the bubble. Let us consider now how $\tilde{\ell}$ varies with $\tilde{R}$: at time t_0 the average bubble radius is $\langle R_0\rangle$ and the total number of bubbles in the sample is n_0. At time $t > t_0$, $\langle R\rangle > \langle R_0\rangle$ and the total number of bubbles in the foam is n. As the gas volume fraction is constant, and neglecting structural changes to the foam, the surface area covered by those bubbles is constant, so we get:

$$\frac{n_0}{n} \sim \left(\frac{\langle R\rangle}{\langle R_0\rangle}\right)^2 = \tilde{R}^2. \tag{6}$$

The total number of disappeared bubbles of initial size $\langle R_0\rangle$ per remaining bubble is therefore:

$$\frac{n_0 - n}{n} \sim \tilde{R}^2 - 1. \tag{7}$$

Assuming that each disappeared bubble provided to the shell an emulsion volume $\varepsilon\pi\langle R_0\rangle^2 d$, volume conservation gives an estimation for $\tilde{\ell}$:

$$\tilde{\ell} \sim \varepsilon\frac{\tilde{R}^2 - 1}{\tilde{R}}. \tag{8}$$

The scaling here is expected to account for the fact that (1) geometrical aspects have been oversimplified, (2) we did not consider the volume of the small bubbles embedded in the shell, (3) the emulsion accumulation process may have started before t_0. Introducing $\tilde{\ell}$ in eqn (5) gives:

$$\frac{1}{\tilde{R}} \sim \mathrm{Bi}\varepsilon\frac{\langle R_0\rangle}{d}\frac{\tilde{R}^2 - 1}{\tilde{R}}. \tag{9}$$

As a result, we can find the normalised radius $\tilde{R}_{ys} = R_{ys}/\langle R_0\rangle$ at which coarsening is stopped by emulsion rheology:

$$\tilde{R}_{ys} \sim \left(1 + \frac{d}{\mathrm{Bi}\varepsilon\langle R_0\rangle}\right)^{1/2}. \tag{10}$$

So we have a scaling for the average radius at which the coarsening process should be stopped by the yield-stress fluid composing the foam continuous phase. We now compare this predicted critical radius to the experimental $\tilde{R}_{sk} = R_{sk}/\langle R_0\rangle$ obtained in Section 3.3, at which coarsening has not stopped but is certainly influenced by the yield stress fluid. Therefore, we expect the predicted radius R_{ys} to be larger than R_{sk}.

The comparison between $\tilde{R}_{sk}$ and $\tilde{R}_{ys}$ is shown in Fig. 7. We observe a linear relation between the two radii, meaning that our model captures the impact of continuous phase rheology, liquid fraction and confinement (*cf.* Fig. S5 in ESI†). We note that the scaling overestimates the datapoints with ϕ = 70% and underestimates the ones for $\phi > 70\%$. We expect this to be the signature of the incomplete description of the foam structure. The prefactor is around 5, which again confirms the validity of the scaling law. We stress that we expect $\tilde{R}_{ys}$ to be larger than $\tilde{R}_{sk}$ as they do not characterise the same moment in the foamed emulsion ageing. It should finally be mentioned that we would experimentally observe this predicted stop in the coarsening only if the foamed emulsion kept an average structure as considered for the model. Yet in our experiments the structure gradually deviates and becomes highly heterogeneous; therefore we observe the foamed emulsion coarsening significantly slowing down but never really stopping.

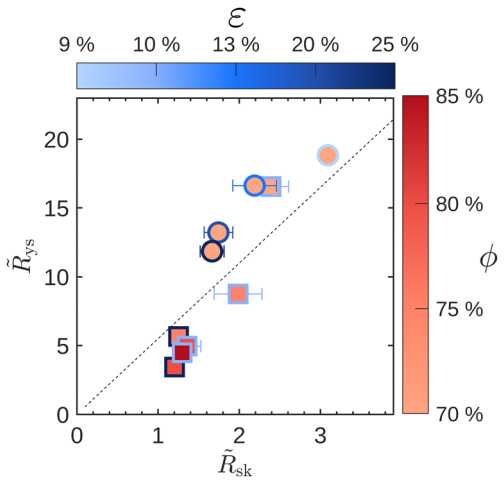

Fig. 7 Normalised theoretical critical radius $\tilde{R}_{ys} = R_{ys}/\langle R_0\rangle$ plotted as a function of the normalised experimental critical radius $\tilde{R}_{sk} = R_{sk}/\langle R_0\rangle$. Here, the slope of the dashed line is 5.5.

4 Conclusion

We studied the coarsening of a quasi-2D foam made from a model yield stress fluid, a concentrated oil-in-water emulsion. We explored the impact of the emulsion oil fraction ϕ, the foam liquid fraction ε and the confining gap d on the foamed emulsion coarsening process. Our experiments show that increasing the yield stress τ_y of the interstitial emulsion leads to slower foam coarsening. This slowing down happens together with an accumulation of small bubbles that induces an increasingly asymmetric bubble size distribution. A high oil fraction ϕ also leads to a significant heterogeneity in the foamed emulsion structure: we find large bubbles separated by very thin Plateau borders and accumulated small bubbles clustered and surrounded by much more liquid. While bigger bubbles keep coarsening, the shrinking rate of smaller bubbles is significantly slowed down by the emulsion stiffness. The impact of the continuous phase rheology is stronger as we increase the amount of yield stress fluid in the foam by making the foam wetter.

We extract a critical radius R_{sk}, which characterises the onset of the structural change in the foamed emulsion. The experiments show that R_{sk} decreases with increasing ϕ, increasing ε, but increases with increasing gap size. To rationalise the variation of R_{sk} with these parameters we consider that an extra

pressure is required to displace the yield stress fluid that had accumulated around the bubbles. This can be used to predict a critical radius for the arrest of coarsening, which we find scales linearly with R_{sk}. This suggests that the resistance of the yield stress fluid is the dominant mechanism through which coarsening is impacted.

The experiments carried out and presented in this paper show highly heterogeneous materials that do not follow Plateau's laws. Understanding how these complex foams coarsen is of great interest for all the applications requiring the solidification of a liquid foam, as the latter will age before solidifying. Moreover the unrelaxed internal structures that result from complex foam ageing will be transferred to the foams once solidified, impacting the mechanical properties of the final material.[45,46] Controlling the structural evolution is then crucial to tune the features of the final foamy material.

Data availability

The videos of the coarsening foams used in this study can be found in the Zenodo database using the following links **https://zenodo.org/records/12680668** (variation of liquid fraction) and **https://doi.org/10.5281/zenodo.7535841** (variation of oil volume fraction).

Conflicts of interest

There are no conflicts to declare.

Acknowledgements

This work was supported by the European Space Agency (ESA) through project Soft Matter Dynamics. The French space agency CNES is acknowledged for the PhD grant of N. Galvani and its support in the frame of the GDR ''Micropesanteur Fondamentale et Appliqué'' with the project ''Hydrodynamics of wet foams''.

Notes and references

1 I. Cantat, S. Cohen-Addad, F. Elias, F. Graner, R. Höhler, O. Pitois, F. Rouyer and A. Saint-Jalmes, *Foams: structure and dynamics*, Oxford University Press, Oxford, 2013.
2 J. Stavans, *Rep. Prog. Phys.*, 1993, **56**, 733.
3 J. Von Neumann, *Metal interfaces*, American Society for Metals, Cleveland, 1952, vol. 108, pp. 108–110.
4 C. Wagner, *Z. Elektrochem.*, 1961, **65**, 581–591.
5 W. Mullins, *J. Appl. Phys.*, 1986, **59**, 1341–1349.
6 D. J. Durian, D. Weitz and D. Pine, *Phys. Rev. A: At., Mol., Opt. Phys.*, 1991, **44**, R7902.
7 J. Lambert, R. Mokso, I. Cantat, P. Cloetens, J. A. Glazier, F. Graner and R. Delannay, *Phys. Rev. Lett.*, 2010, **104**, 248304.
8 W. W. Mullins, *J. Appl. Phys.*, 1956, **27**, 900–904.
9 J. A. Glazier, S. P. Gross and J. Stavans, *Phys. Rev. A: At., Mol., Opt. Phys.*, 1987, **36**, 306–312.
10 J. Stavans, *Phys. Rev. A: At., Mol., Opt. Phys.*, 1990, **42**, 5049–5051.
11 R. Prud'homme and S. Khan, *Foams: Theory, Measurements, and Applications*, Marcel Dekker Inc., New York, 1996, vol. 57.
12 D. Weaire and S. Hutzler, *The Physics of Foams*, Oxford University Press, Oxford, 1999.
13 A. Saint-Jalmes, D. Durian and D. Weitz, *Kirk-Othmer Encyclopedia of Chemical Technology*, Wiley, 2005.
14 S. Cohen-Addad, R. Höhler and Y. Khidas, *Phys. Rev. Lett.*, 2004, **93**, 028302.
15 M. Le Merrer, S. Cohen-Addad and R. Höhler, *Phys. Rev. Lett.*, 2012, **108**, 188301.
16 S. Cohen-Addad, R. Höhler and O. Pitois, *Annu. Rev. Fluid Mech.*, 2013, **45**, 241–267.
17 F. Gorlier, Y. Khidas and O. Pitois, *J. Rheol.*, 2017, **61**, 919–930.
18 H. Bey, F. Wintzenrieth, O. Ronsin, R. Hohler and S. Cohen-Addad, *Soft Matter*, 2017, **13**, 6816–6830.
19 N. Dubash and I. Frigaard, *J. Non-Newtonian Fluid Mech.*, 2007, **142**, 123–134.
20 D. Sikorski, H. Tabuteau and J. Bruyn, *J. Non-Newtonian Fluid Mech.*, 2009, **159**, 10–16.
21 I. Lesov, S. Tcholakova and N. Denkov, *J. Colloid Interface Sci.*, 2014, **426**, 9–21.
22 G. Samson, A. Phelipot-Mardelé and C. Lanos, *Mag. Concr. Res.*, 2017, **69**, 201–216.
23 C. Arriagada, I. Navarrete and M. Lopez, *Constr. Build. Mater.*, 2019, **228**, 116746.
24 A. Salonen, *Curr. Opin. Colloid Interface Sci.*, 2020, **50**, 101381.
25 O. Okesanjo, G. Aubry, S. Behrens, H. Lu and J. C. Meredith, *Lab Chip*, 2023, **23**, 4434–4444.
26 Y. Si, J. R. Royer, T. Li and P. S. Clegg, *J. Colloid Interface Sci.*, 2023, **646**, 671–678.
27 A. Salonen, R. Lhermerout, E. Rio, D. Langevin and A. Saint-Jalmes, *Soft Matter*, 2012, **8**, 699–706.
28 C. Guidolin, J. Mac Intyre, E. Rio, A. Puisto and A. Salonen, *Nat. Commun.*, 2023, **14**, 1125.
29 J. Goyon, F. Bertrand, O. Pitois and G. Ovarlez, *Phys. Rev. Lett.*, 2010, **104**, 128301.
30 W. Kloek, T. van Vliet and M. Meinders, *J. Colloid Interface Sci.*, 2001, **237**, 158–166.
31 D. C. Venerus, *J. Non-Newtonian Fluid Mech.*, 2015, **215**, 53–59.
32 L. Ducloué, O. Pitois, J. Goyon, X. Chateau and G. Ovarlez, *J. Non-Newtonian Fluid Mech.*, 2015, **215**, 31–39.
33 T. Gaillard, M. Roché, C. Honorez, M. Jumeau, A. Balan, C. Jedrzejczyk and W. Drenckhan, *Int. J. Multiphase Flow*, 2017, **96**, 173–187.
34 H. M. Princen and A. Kiss, *J. Colloid Interface Sci.*, 1986, **112**, 427–437.
35 T. Mason, J. Bibette and D. Weitz, *J. Colloid Interface Sci.*, 1996, **179**, 439–448.
36 N. Politova, S. Tcholakova, Z. Valkova, K. Golemanov and N. D. Denkov, *Colloids Surf., A*, 2018, **539**, 18–28.

37 A. E. Roth, C. D. Jones and D. J. Durian, *Phys. Rev. E: Stat., Nonlinear, Soft Matter Phys.*, 2013, **87**, 042304.
38 N. Isert, G. Maret and C. M. Aegerter, *Eur. Phys. J. E: Soft Matter Biol. Phys.*, 2013, **36**, 116.
39 J. A. Glazier and J. Stavans, *Phys. Rev. A: At., Mol., Opt. Phys.*, 1989, **40**, 7398–7401.
40 C. D. Schimming and D. J. Durian, *Phys. Rev. E*, 2017, **96**, 032805.
41 C. Gay, P. Rognon, D. Reinelt and F. Molino, *Eur. Phys. J. E: Soft Matter Biol. Phys.*, 2011, **34**, 1–11.
42 N. Galvani, M. Pasquet, A. Mukherjee, A. Requier, S. Cohen-Addad, O. Pitois, R. Höhler, E. Rio, A. Salonen, D. J. Durian and D. Langevin, *Proc. Natl. Acad. Sci. U. S. A.*, 2023, **120**, e2306551120.
43 C. Guidolin, PhD thesis, Université Paris-Saclay, 2022.
44 A. J. Webster and M. E. Cates, *Langmuir*, 2001, **17**, 595–608.
45 S. Heitkam, W. Drenckhan, T. Titscher, D. Weaire, D. C. Kreuter, D. Hajnal, F. Piechon and J. Fröhlich, *Eur. J. Mech. A Solids*, 2016, **59**, 252–264.
46 M. Jouanlanne, A. Egelé, D. Favier, W. Drenckhan, J. Farago and A. Hourlier-Fargette, *Soft Matter*, 2022, **18**, 2325–2331.